16

Electronic structure and non-linear optical properties of superlattices based on quartz and silicon

© E.M. Roginskii[1], M.B. Smirnov[2], D.V. Pankin[2], A.V. Savin[1]

[1] Ioffe Institute,
St. Petersburg, Russia
[2] St. Petersburg State University,
St. Petersburg, Russia

E-mail: e.roginskii@mail.ioffe.ru

Received October 18, 2024
Revised October 28, 2024
Accepted October 29, 2024

The structural, electronic and non-linear properties of the superlattices based on quartz and silicon are studied in a framework of quantum-chemistry ab initio calculations. The thermodynamic stability of the structure is established and analysis of electronic and optical properties is carried out. The values of band offsets is obtained using quasi-particle GW approach. The values reproduce quite well experimental data and equal to 3.87 and 3.14 eV for valence and conducting zones respectively. The nonlinear properties and an influence of layers thickness on linear and quadratic dielectric susceptibility is established. The strongest nonlinear response in the structure with double silicon layered is revealed.

Keywords: supercell nonlinear optics quantum chemistry.

DOI: 10.61011/PSS.2024.11.60114.268

1. Introduction

Currently, there is an explosive interest in the problem of finding new functional materials in the world. Silicon is broadly used in microelectronics and the chemical industry. It is mostly found in cubic modification, due to its widespread distribution in the earth's crust. Silicon has a unique combination of structural, chemical, and electronic properties. It is known that the band gap of the cubic phase is 1.12 eV [1,2], which makes it possible to use this material as the main elements of solar panels. However, the features of the zone structure do not allow achieving the maximum efficiency of such solar cells. This circumstance initiates the search for new structural modifications with optimal characteristics for specific technological tasks. In particular, the theoretical prediction of thermodynamically stable silicon structures is relevant because of the complexity and expensive cost of synthesizing new materials [3–7].

The simplest chemical compound with silicon is oxide, which is also common on earth and has a very rich family of polymorphs, which structurally differ mainly in packing tetrahedra SiO_2 into a periodic crystalline structure or into an amorphous state. The most prominent representative of silica is quartz, which is a wide-band dielectric with a direct optical transition. The significant difference of the electronic structure of silicon and its oxide allows expecting a unique combination of fundamental properties as a result of the fusion of the two materials.

The development of technology in the last decade has led to the possibility of growing nanoscale structures, in particular short-period superlattices, which are layered heterostructures in which layers of one substance alternate with layers of another isomorphic material. Such a fusion of materials results in an overlap of wave functions and the occurrence of a gap in energy levels at the interface boundaries. Studying the gap of bands is one of the key problems, since the size of the gap determines the physical properties of the heterostructure that are important for creating electronic [8] or optoelectronic devices [9]. There are many theoretical approaches to the study of the electronic structure of heterostructures, among which a significant share is occupied by calculations within the framework of density functional theory.

This paper primarily presents the results of study of the structural properties of superlattices obtained by intergrowing of cubic silicon with quartz. Such structures have shown thermodynamic stability and variation of electronic and optical properties depending on the thickness of the layers.

2. Calculation technique

The calculations based on the first principles were carried out within the framework of the density functional theory using ABINIT program [10,11]. The calculations used functionals, the exchange-correlation part of which was described in the approximation of the local density LDA [12]. Optimized non-local (with two projectors of the non-local part), norm-conserving pseudopotentials for Si and O atoms were used in these calculations [13]. The electrons in the orbitals $2s2p$ for the O atom and $3s3p$ for the Si atom

were considered as valence in the calculations. The cut-off energy in the calculation of the electronic structure was 40 Ha. The Monkhorst-Pack grids [14] were used for integration over the Brillouin zone in size $6 \times 6 \times 2$. The calculations involved complete relaxation of both atomic positions and lattice parameters. Relaxation was carried out until the forces acting on the atoms became less than $2 \cdot 10^{-5}$ Ha/Bohr with a self-consistent calculation of the total energy with an accuracy better than 10^{-8} Ha, and the deviation from zero pressure did not exceed 0.1 Kbar.

The electronic structure and dielectric permittivity were calculated using the quasi-particle approximation G_0W_0 [15]. The wave functions and energy eigenvalues found in the generalized gradient approximation (GGA) were used as input data. The dielectric matrix $\varepsilon_{GG'}(q, \omega)$ was calculated on a grid of 48 points from the polarizability matrix $P_{GG'}(q, \omega)$ calculated in the random phase approximation (RPA) for 56 filled and 250 unfilled zones. Dynamic shielding was described by the single-pole Godby-Needs plasmon model. The calculations used Fourier components of wave functions with a maximum kinetic energy of 35 Ha. The corrections to the energies found in the GGA approximation were calculated as diagonal matrix elements of the operator $[\Sigma - E_{xc}]$, where $\Sigma = GW$ is the self-energy operator, E_{xc} is the exchange-correlation energy operator, G is the Green's function, and $W = [\varepsilon^{-1}\upsilon]$ is the operator of the shielded Coulomb interaction. The wave function components with kinetic energy up to 35 Ha were used when calculating Σ for both the exchange and correlation parts.

3. Structural properties

Superlattices were constructed in this study by intergrowing bulk silicon (space group $Fd3m$) with quartz ($P3_221$) in such a way that the silicon plane (001) was parallel to the quartz plane (120). Figure 1 shows a scheme for the formation of a superlattice $(Si)_m/(SiO_2)_n$ for $m = n = 1$ (1×1) formed by alternating layers of silicon and quartz with a thickness equal to one period of the unit cell of bulk materials (Figure 1, *b*). The atoms in such a superlattice form a structure with the space group $P222_1$, and the atoms of the silicon layer occupy highly symmetric Wyckoff positions 2*a*, 2*c* and 2*d* with local symmetry 2, and in the oxide layer positions 2*b* and 2*c*, while the interface layer is filled with silicon atoms in the general Wyckoff position 4*e*. Oxygen atoms are located in highly symmetric positions 4*d* and common 4*e*, which is typical for quasi-molecular crystals [16].

The structural parameters of the superlattice obtained after optimization of the geometry showed that in the interface plane, the oxide layer experiences a tensile strain (6.5%), and the silicon layer a compression strain (1%), while the energy of formation of the superlattice is 2.55 eV/Si. The superlattice considered in this paper has greater mechanical stability and an energetically more favorable configuration compared with the structure studied earlier in Ref. [17,18] (formation energy 3.74 eV). The structural parameters of the studied superlattices and bulk precursors are listed in Table 1. The table shows a good agreement between the calculations and the experiment for bulk precursors, which indicates the adequacy of the chosen calculation scheme.

The resulting superlattice configuration was also tested for stability with respect to phonon states. Figure 2 shows the calculated dispersion of phonon states along highly symmetric directions in the Brillouin zone.

As can be seen from the figure, there are no states with imaginary frequencies throughout the BZ, and therefore the structure is stable while maintaining orthorhombic symmetry. Moreover, as can be seen from the partial density of vibrational states, the main contribution to low-frequency vibrational states (with frequency up to 400 cm^{-1}) is made by silicon atoms localized in the silicon layer, while the atoms of the oxide layer make the greatest contribution to states with a frequency greater than 400 cm^{-1}, which indirectly indicates the presence of localized oscillations in a separate layer in the superlattice.

The vibrational states of the superlattices 2×1 and 1×2 were studied only in the Γ-point of the ZB due to the significant resource consumption of calculation of the dispersion of phonon branches. It is necessary to expect the absence of the occurrence of imaginary modes for superlattices of a longer period because the increase of the period along the SL growth axis leads to a collapse of the ZB in this direction.

4. Electronic structure and dielectric properties

As is known, the electronic states in periodic structures are determined not only by the composition, but also by the structural ordering in the crystal lattice. The experimental value of the band gap (E_g) of quartz is 8.9 eV [20], and a similar value for bulk silicon is 1.12 eV [21] (for a direct optical transition), a significant difference of the magnitude of E_g suggests that it is possible to adjust the band gap to the required value in a wide range (from ultraviolet to infrared spectrum) of length waves by varying the composition of the superlattice. The electronic band structure shown in Figure 3 was calculated in the quasi-particle approximation G_0W_0 for revealing the impact of spatial structure on electronic states.

Figure 3 shows that, unlike bulk silicon, the superlattice is a direct-band semiconductor with a band gap of 1.82 eV, which is quite close to the Shockley-Queisser limit, which determines the maximum efficiency of a solar cell. At the same time, the value of the effective mass of electrons calculated by numerical differentiation $m^*_{h,e} = \hbar^2\left[\frac{\partial^2 E}{\partial k^2}\right]^{-1}$ was $m^*_e \sim 0.23m_e$, which is about two times less than the value of the effective mass of holes $m^*_e \sim 0.48m_e$. The obtained values are slightly lower than the effective masses in silicon oxide, which are $0.42m_e$ and $0.58m_e$ [22] for

Table 1. Lattice parameters and atomic coordinates in Si/SiO_2 SL and precursors

	Si-bulk		SiO_2		CP Si/SiO_2
Parameter	Experiment[1]	Calculation	Experiment[1]	Calculation	Settlement
			Lattice parameters		
a, Å	5.430	5.468	4.913	4.951	5.276
b, Å	5.430	5.468	4.913	4.951	5.450
c, Å	5.430	5.468	5.405	5.443	12.267
			Positions of atoms, relative units		
Si1	(0,0,0)	(0,0,0)	(0.469,0,0.667)	(0.471,0,0.667)	(0.000,0.333,0.500)
Si2					(0.250,0.000,0.652)
Si3					(0.000,0.236,0.000)
Si4					(0.250,0.500,0.908)
Si5					(0.750,0.000,0.899)
Si6					(-0.039,0.702,0.811)
$O1_1$			(0.414,0.268,0.785)	(0.413,0.265,0.787)	(0.250,0.500,0.479)
$O2_1$					(0.750,0.500,0.775)
$O3_1$					(0.446,0.841,0.589)
$O4_1$					(0.090,0.811,0.716)

Note. [1] Parameters from Ref. [19].

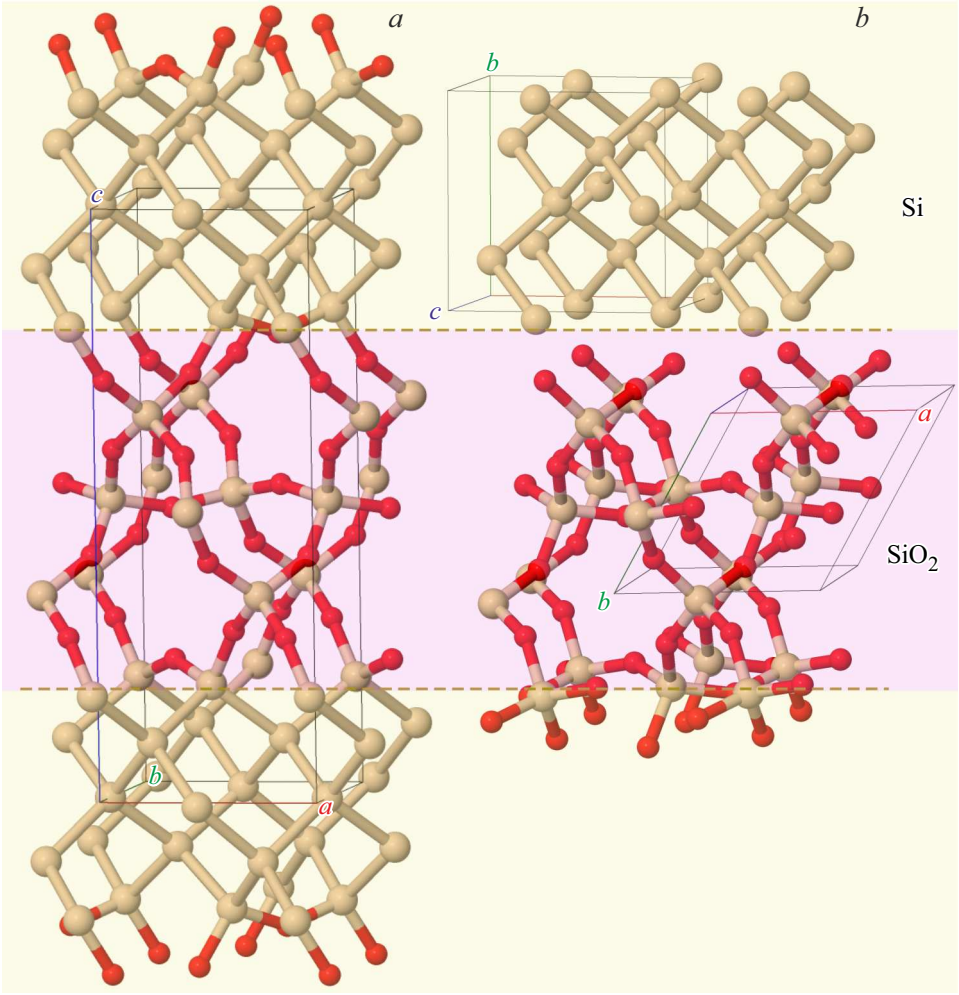

Figure 1. Unitcell cell of superlattice Si/SiO_2 (*a*) and cells of bulk precursors (*b*). Large beige balls are silicon atoms, small red balls are oxygen atoms.

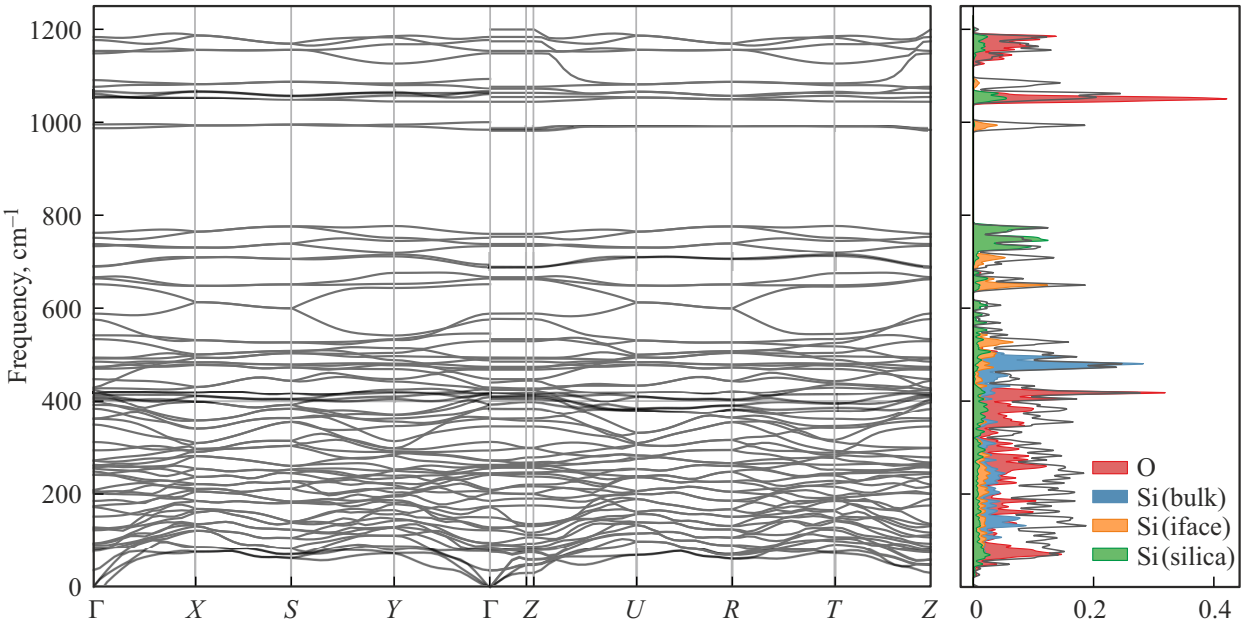

Figure 2. Dispersion of phonon states of superlattice Si/SiO_2 (left) along the symmetry directions of the BZ and the partial density of phonon states (on the right).

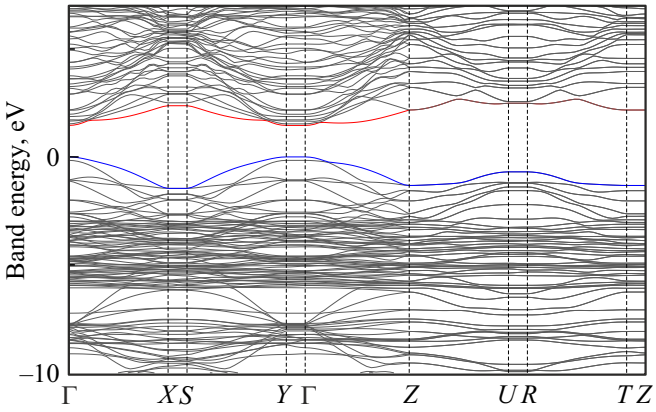

Figure 3. Band structure of Si/SiO_2 superlattice calculated by the G_0W_0 method.

electrons and holes, respectively, and therefore the carrier mobility in the superlattice is higher. However, it is worth noting the high anisotropy of the effective mass tensor, — perpendicular to the interface due to the degeneration of the dispersion of electronic states, the mass values acquire high values that have no physical meaning.

The density of electronic states projected onto individual atoms was calculated to analyze the states of the valence band and the conduction band (Figure 4).

It can be concluded from the analysis of the density of states that the greatest contribution to the high-energy branches of the valence band is made by Si atoms in the silicon and interface layers (Figure 4, *a, b*), with the most significant contribution made by electrons of $3p$-orbitals. The bottom of the conduction band is also formed by electrons of silicon atoms, but this time the contribution is made by electrons $4s$, $4p$, $3d$, which form virtual states in free atoms.

It is worth noting that the energy levels of the Si and O atoms of the oxide layer (Figure 4, *c, d*) located quite deep in the valence band and high in the conduction band, so optical transitions in the superlattice are mainly determined by electronic states in the silicon layer. Such a structure indicates the presence of a gap between the valence band and the conduction band in layers of different compositions.

It is known that the gap of the valence band of the heterostructure is found by the following formula [23]:

$$\Delta E_v = (E_v^{\mathrm{Si}} - E_v^{\mathrm{SiO_2}}) + \Delta V, \qquad (1)$$

where ΔV is the difference of the averaged electrostatic potential in different layers of the heterostructure, which is obtained from calculations of the long-period superlattice. Obviously, the gap in the conduction band is related to the gap in the valence band by the ratio:

$$\Delta E_c = (E_g^{\mathrm{Si}} - E_g^{\mathrm{SiO_2}}) + \Delta E_v, \qquad (2)$$

where E_g^{Si} and $E_g^{\mathrm{SiO_2}}$ are the band gap values of bulk silicon and oxide, respectively. It is worth noting that the fields of elastic deformations resulting from the fusion of layers into a single structure are not isotropic, which leads to a decrease of the cubic symmetry of bulk silicon to tetragonal.

The zone discontinuities were calculated at the first stage within the framework of the density functional theory, then, using the Kohn-Sham orbitals, quasi-particle corrections were calculated using the G_0W_0 method, as schematically shown in Figure 5.

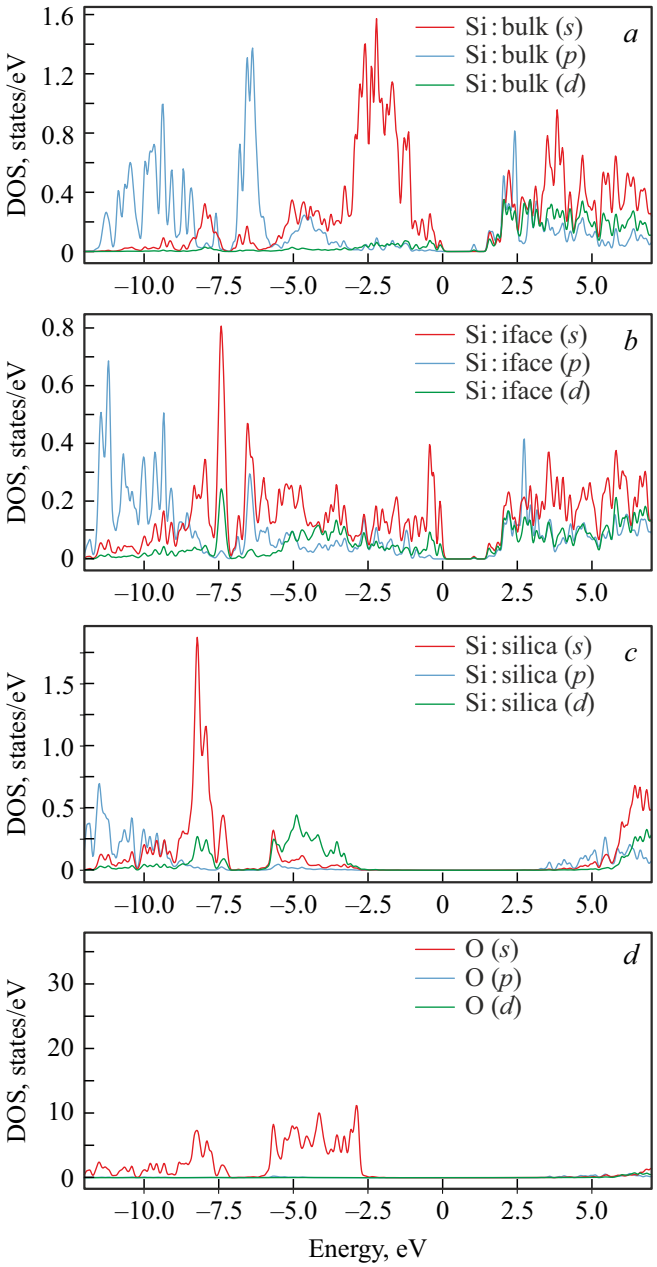

Figure 4. Projections of the density of electronic states of Si/SiO_2 superlattice onto Si atomic orbitals in the silicon layer (a), in the interface layer (b) and the oxide layer (c) and on orbitals of atoms O (d).

The calculation showed that the quasi-particle corrections for the SiO_2 layer shift the levels of the valence bands and conduction bands in the opposite direction by approximately the same amount on the order of 1.3 eV, summing up the band gap by 2.75 eV. The valence band almost does not change position in the silicon layer, only the conduction band shifts by 0.68 eV. As a result, the displacement values of the zones $\Delta E_v = 3.87$ eV and $\Delta E_c = 3.14$ eV are calculated, which is in good agreement with experimental data of 4.3 and 3.1 eV, respectively [24]. Thus, taking into account quasi-particle effects turns out to be critically important when calculating the electronic structure of Si/SiO_2 superlattices, and the calculation results are in good agreement with experimental data.

Table 2. Calculated band gap and dielectric properties of $(Si)_m(SiO_2)_n$ $(m \times n)$ SL and precursors

	E_g^{GW}, eV	$\chi_{xx}^{(1)}$	$\chi_{zz}^{(1)}$	$\chi^{(2)}$, pm/V
Si-strain	0.77	16.01	16.01	0
SiO_2	8.56	1.468	1.468	0.845
SL 1 × 2	2.12	3.16	3.16	0.172
SL 1 × 1	1.83	4.3	4.3	0.106
SL 2 × 1	1.28	5.94	5.94	3.616
SL 2 × 2	1.30	5.45	5.45	1.95

Calculations of the electronic structure of superlattices with increased layer thicknesses were also performed, and the band gap widths are shown in Table 2.

As can be seen from Table 2, the band gap is expected to increase as the thickness of the silicon layer increases, however, if the thicknesses of the layers increase by the same multiplicity, the value of E_g decreases by 30%, which indicates a decrease of the overlap of the wave functions of adjacent layers. In other words, the thick layers retain the individual characteristics of the bulk precursors and interact weakly with each other. In general, the expected pattern of the effect of the superlattice composition on the band gap is observed in the range from 1.3 to 2.1 eV, which corresponds to the wavelength range from 600 to 950 nm, i. e. the region of maximum solar radiation. Thus, the studied structures are of interest for use in optical devices in which dielectric properties play an important role.

Calculations of linear and quadratic nonlinear susceptibility were performed within the framework of perturbation theory, and the results are shown in Table 2. There is a fairly strict correlation between the value of the dielectric constant and the band gap; the linear susceptibility rapidly decreases with the increase of the latter, reaching a minimum in the case of quartz (the table below shows the average value of the dielectric susceptibility in three directions).

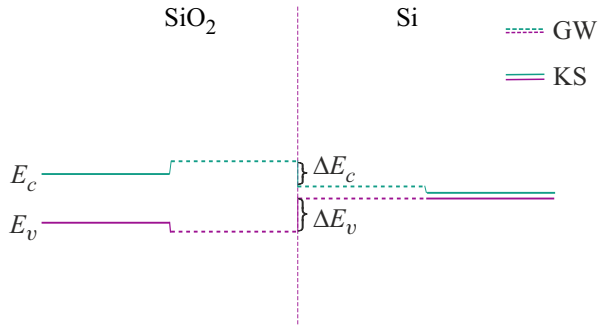

Figure 5. Illustration to the zone gap calculation scheme. Solid lines — levels calculated in the GGA approximation, dotted lines — adjusted G_0W_0.

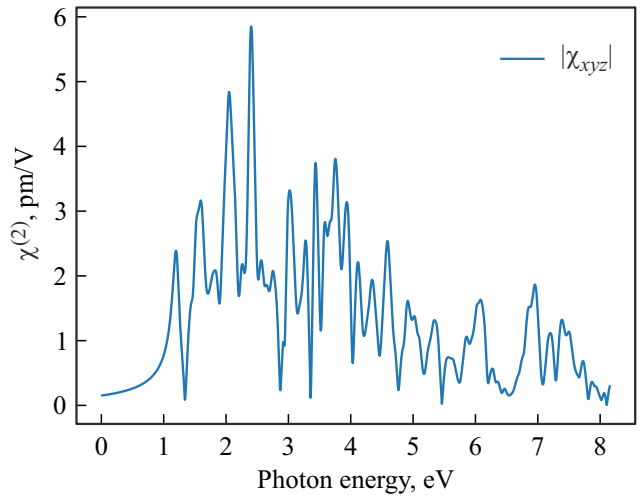

Figure 6. Dispersion dependence of the second harmonic generation coefficient of Si/SiO_2 1×1 SL.

In the case of nonlinear dielectric susceptibility, the connection is not so obvious because of the dependence of nonlinear properties on the symmetry of the crystal lattice. So, in the case of bulk silicon, the generation of the second harmonic is prohibited by the selection rules, and all components of the tensor $\chi^{(2)}_{ijk}$ are zero in the static approximation. The selection rules allow only two nonzero components for quartz — $\chi^{(2)}_{xxx}$ and $\chi^{(2)}_{xyy}$, which are equal in magnitude but opposite in sign, the calculated value is given in Table 2. The obtained value correlates with experimental data for amorphous silicon used as a waveguide on an industrial scale.

Superlattices with a thin silicon layer exhibit rather weak nonlinear properties. According to the selection rules, the quadratic nonlinear susceptibility tensor of the third rank $\chi^{(2)}$ of structures with space group $P222_1$ has only one allowed component, namely $\chi^{(2)}_{xyz}$. Calculations show that this value dramatically increases with the increase of the thickness of the silicon layer, several times higher than the values for quartz, which opens up opportunities for the use of this material in industry.

The dispersion dependence of the quadratic nonlinear dependence plotted in Figure 6 was also calculated in this paper.

It is worth noting the strong dispersion dependence of the nonlinear response, which dramatically increases with the increase of the light source wavelength. For example, the magnitude of the nonlinear susceptibility is 3.3 pm/V in the case of second harmonic generation at a frequency of 620 nm, which is ten times higher than the static value. Unfortunately, the calculation of the dynamic nonlinear properties of SL with thicker layers is limited by computational resources, however, the great potential of these structures in the field of nonlinear optics can be inferred even from the example of 1×1 SL.

5. Conclusion

The results of a comprehensive study of the structural, electronic, and dielectric properties of Si/SiO_2 superlattices are presented in this paper. The band structure, spatial structure, phonon spectra, and nonlinear optical susceptibility of a series of silicon oxide superlattices with different layer thicknesses have been studied using nonempirical quantum mechanical methods. A model based on a combination of crystalline silicon and quartz lattices is used to describe the interface structure. It is shown that a thermodynamically stable heterostructure can be formed with minor deformations of both lattices. The values of the band shift in the heterojunction region were obtained, including taking into account the corrections calculated using the quasiparticle approximation GW, which amounted to 3.87 and 3.14 eV, for the valence band and the conduction band, respectively, which is in good agreement with experimental data. The nonlinear optical properties of superlattices and the effect of layer thickness on linear and quadratic dielectric susceptibility have been studied. It is shown that the maximum nonlinear response is achieved in materials with a silicon layer with a thickness of two lattice cells. The authors hope to arouse interest in the experimental study of nonlinear optical properties of superlattices based on silicon and its oxide.

Acknowledgments

The calculations presented in this paper were partially performed using the computing resources of the Joint Supercomputer Center of the Russian Academy of Sciences, and using the computing resources of the supercomputer of Ioffe Institute of Physics and Technology.

Funding

The study was supported by a grant from the Russian Science Foundation (No. 22-22-20021) and a grant from the St. Petersburg Science Center (No. 32/2022).

Conflict of interest

The authors declare that they have no conflict of interest.

References

[1] Y. Okada, Y. Tokumaru. J. Appl. Phys. **56**, 314 (1984).
[2] A.G. Cullis, L.T. Canham, P.D.J. Calcott. J. Appl. Phys. **82**, 909 (1997).
[3] K. Takeda, K. Shiraishi. Phys. Rev. B **50**, 14916 (1994).
[4] G.G. Guzmán-Verri, L.C. Lew Yan Voon. Phys. Rev. B **76**, 075131 (2007).
[5] Q. Wang, B. Xu, J. Sun, H. Liu, Z. Zhao, D. Yu, C. Fan, J. He. J. Am. Chem. Soc. **136**, 9826 (2014).
[6] A. Mujica, C.J. Pickard, R.J. Needs. Phys. Rev. B **91**, 214104 (2015).

[7] R. Tutchton, C. Marchbanks, Z. Wu. Phys. Rev. B **97**, 205104 (2018).
[8] G.D. Wilk, R.M. Wallace, J.M. Anthony. J. Appl. Phys. **89**, 5243 (2001).
[9] A.C. Morteani, P. Sreearunothai, L.M. Herz, R.H. Friend, C. Silva. Phys. Rev. Lett. **92**, 247402 (2004).
[10] X. Gonze, B. Amadon, P.-M. Anglade, J.-M. Beuken, F. Bottin, P. Boulanger, F. Bruneval, D. Caliste, R. Caracas, M. Côté, T. Deutsch, L. Genovese, P. Ghosez, M. Giantomassi, S. Goedecker, D. Hamann, P. Hermet, F. Jollet, G. Jomard, S. Leroux, M. Mancini, S. Mazevet, M. Oliveira, G. Onida, Y. Pouillon, T. Rangel, G.-M. Rignanese, D. Sangalli, R. Shaltaf, M. Torrent, M. Verstraete, G. Zerah, J. Zwanziger. Comput. Phys. Commun. **180**, 2582 (2009).
[11] X. Gonze, G. Rignanese, M. Verstraete, J. Beuken, Y. Pouillon, R. Caracas, F. Jollet, M. Torrent, G. Zerah, M. Mikami, P. Ghosez, M. Veithen, J.-Y. Raty, V. Olevano, F. Bruneval, L. Reining, R. Godby, G. Onida, D. Hamann, D. Allan. Zeitschrift für Kristallographie. Crystalline Materials **220**, 558 (2005).
[12] J.P. Perdew, Y. Wang. Phys. Rev. B **45**, 13244 (1992).
[13] D.R. Hamann. Phys. Rev. B **88**, 085117 (2013).
[14] H.J. Monkhorst, J.D. Pack. Phys. Rev. B **13**, 5188 (1976).
[15] G. Onida, L. Reining, A. Rubio. Rev. Mod. Phys. **74**, 601 (2002).
[16] Y.E. Kitaev, A.G. Panfilov, V.P. Smirnov, P. Tronc. Phys. Rev. E **67**, 011907 (2003).
[17] M.B. Smirnov, D.V. Pankin, E.M. Roginsky, A.V. Savinyu. FTT **64**, 1701 (2022).
[18] M. Smirnov, E. Roginskii, A. Savin, N. Mazhenov, D. Pankin. Coatings **13**, 1231 (2023).
[19] Y. Le Page, G. Donnay. Acta Crystallographica Section B Structural Crystallography and Crystal Chemistry **32**, 2456 (1976).
[20] R.B. Laughlin. Phys. Rev. B **22**, 3021 (1980).
[21] R.J. Van Overstraeten, R.P. Mertens. Solid-State Electron. **30**, 1077 (1987).
[22] R.K. Chanana. Transactions on Machine Learning and Artificial Intelligence **11**, 172 (2023).
[23] R. Shaltaf, G.-M. Rignanese, X. Gonze, F. Giustino, A. Pasquarello. Phys. Rev. Lett. **100**, 186401 (2008).
[24] V.V. Afanas'ev, M. Houssa, A. Stesmans, M.M. Heyns. Appl. Phys. Lett. **78**, 3073 (2001).

Translated by A.Akhtyamov